Cell PRESS
Structure
Article

The WSXWS Motif in Cytokine Receptors Is a Molecular Switch Involved in Receptor Activation: Insight from Structures of the Prolactin Receptor

Robert Dagil,[1,6] Maiken J. Knudsen,[1,6] Johan G. Olsen,[1] Charlotte O'Shea,[1] Magnus Franzmann,[1,2] Vincent Goffin,[3,4] Kaare Teilum,[1] Jens Breinholt,[5] and Birthe B. Kragelund[1,*]

[1]Structural Biology and NMR Laboratory, Department of Biology, University of Copenhagen, Ole Maaloes Vej 5, DK-2200 Copenhagen, Denmark
[2]Department of Biotechnology, Aalborg University, 9000 Aalborg, Denmark
[3]INSERM U845, Centre de Recherche "Croissance et Signalisation," Equipe "Physiopathologie des hormones PRL/GH," F-75015 Paris, France
[4]Université Paris Descartes, Sorbonne Paris Cité, Faculté de Médecine, Site Necker, F-75015 Paris, France
[5]Novo Nordisk A/S, Novo Nordisk Park, 2760 Måløv, Denmark
[6]These authors contributed equally to this work
*Correspondence: bbk@bio.ku.dk
DOI 10.1016/j.str.2011.12.010

SUMMARY

The prolactin receptor (PRLR) is activated by binding of prolactin in a 2:1 complex, but the activation mechanism is poorly understood. PRLR has a conserved WSXWS motif generic to cytokine class I receptors. We have determined the nuclear magnetic resonance solution structure of the membrane proximal domain of the human PRLR and find that the tryptophans of the motif adopt a T-stack conformation in the unbound state. By contrast, in the hormone bound state, a Trp/Arg-ladder is formed. The conformational change is hormone-dependent and influences the receptor-receptor dimerization site 3. In the constitutively active, breast cancer-related receptor mutant PRLR^{I146L}, we observed a stabilization of the dimeric state and a change in the dynamics of the motif. Here we demonstrate a structural link between the WSXWS motif, hormone binding, and receptor dimerization and propose it as a general mechanism for class 1 receptor activation.

INTRODUCTION

The prolactin receptor (PRLR) is a member of the cytokine receptor superfamily. Cytokine receptors are divided into three parts: (1) an extracellular N-terminal domain (ECD) forming two fibronectin type III (FNIII) domains, an N-terminal, membrane-distal domain termed D1 and a membrane-proximal domain, D2; (2) a single transmembrane α-helical segment; and (3) the C-terminal intracellular domain (ICD), which is structurally uncharacterized, containing binding sites for various protein partners involved in intracellular signaling, including Janus kinase 2 (JAK2) (Goffin et al., 2002; Rui et al., 1994).

The primary roles of the PRL/PRLR complex involve stimulation of lactation in the nursing female and the development of breast epithelium during pregnancy (Neville et al., 2002). In males, it participates in the growth and differentiation of the prostate (Goffin et al., 2011; Nevalainen et al., 1997; Robertson et al., 2003). PRL/PRLR has been linked to stimulation of tumor growth with elevated PRL and/or PRLR levels (Carver et al., 2009; Clevenger et al., 2009). This has precipitated extensive pharmaceutical work on the development of PRLR antagonists (Goffin et al., 2005). Genetic analyses of patients presenting with benign or malignant breast tumors have recently revealed the existence of two PRLR alleles encoding missense receptor variants, hPRLR^{I76V} and hPRLR^{I146L} (Bogorad et al., 2008; Canbay et al., 2004; Courtillot et al., 2010; Vaclavicek et al., 2006). Functional analyses showed both variants to be active in the absence of hormone, with hPRLR^{I146L} the most potent. Its biological activity was considered relevant, as hPRLR^{I146L} activated both JAK2/STAT5 and MAPK-pathways; it activated a PRL target reporter gene, promoted autonomous breast cancer cell proliferation, and immortalized Ba/F3 immune cells (Bogorad et al., 2008; Courtillot et al., 2010). The I146L variant was not found in the control cohorts of the epidemiological studies, suggesting its potential involvement in breast pathogenesis.

PRL is a four-helix bundle protein (Teilum et al., 2005) that activates its cognate receptor by forming an asymmetric ternary complex binding two identical receptor molecules (Broutin et al., 2010; van Agthoven et al., 2010). Atomic models of 1:1 and 1:2 complexes of PRL (and derivatives thereof) and PRLR-ECD are available (Broutin et al., 2010; Kulkarni et al., 2010; Svensson et al., 2008; van Agthoven et al., 2010), which characterize the details of the hormone/receptor interfaces, as well as of the receptor-receptor interaction site 3, Figure 1A. The two hormone-receptor interfaces are referred to as sites 1 and 2 with site 1 binding with nM affinity, and site 2 more weakly in the μM range (Jomain et al., 2007). The PRL binding sites involve both D1 and D2. The PRLR-D2 participates in hormone-binding, mainly via Trp139, which is located in loop-L5 (Broutin et al., 2010), here referred to as the binding-loop. The structure of the 2:1 complex has furthermore revealed that the two receptors interact via contacts between the D2 domains. This interface is referred to as site 3.

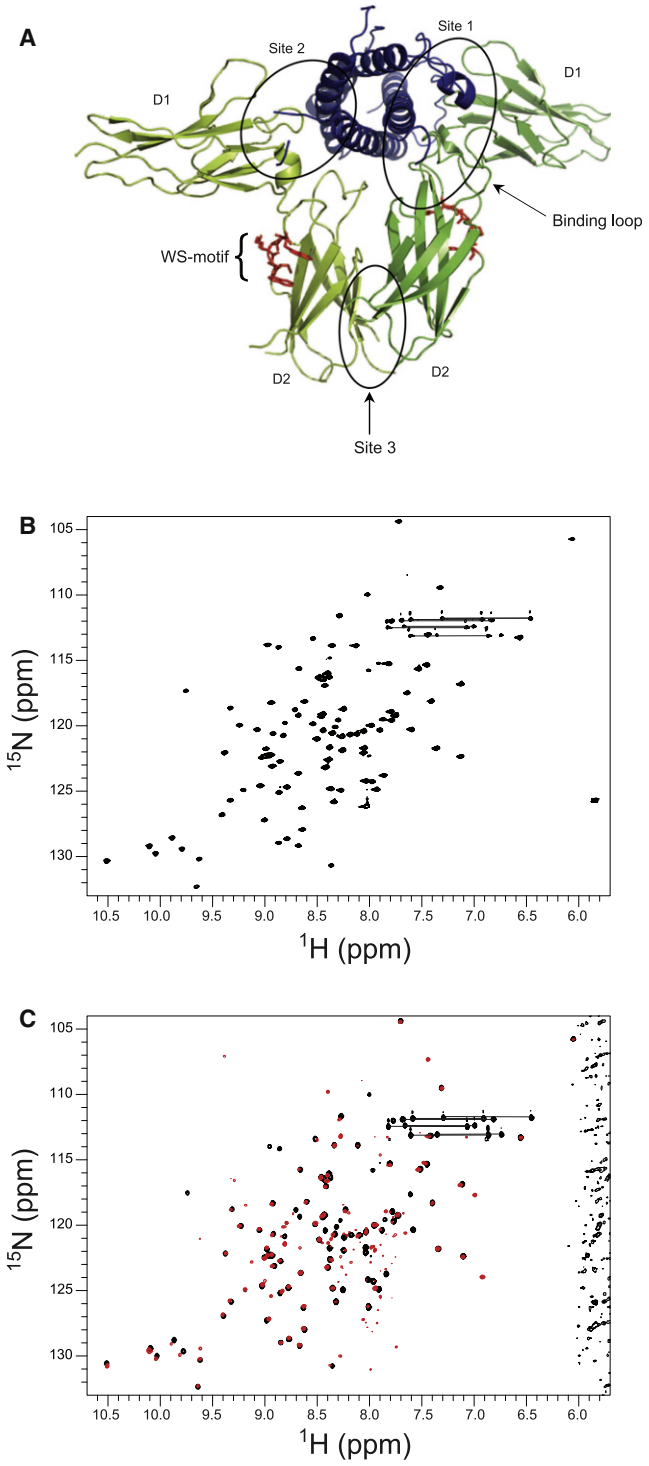

Figure 1. Structure and Spectroscopic Data on hPRLR-ECD

(A) Structure of the 2:1 complex between hPRL and the ECDs of two rPRLRs (van Agthoven et al., 2010). The ECDs, shown in green, each consists of two FNIII domains, D1 and D2. The hormone in blue primarily binds to D1 with the bulk of the interface buried in site 1. The WS motif is shown in red.

(B) The [^{15}N,^{1}H]-HSQC spectrum of hPRLR-D2 shows a large dispersion in the proton dimension indicative of a folded, globular domain. Asn and Gln side chains peaks are linked by solid lines. The spectrum was recorded on 0.5 mM ^{13}C,^{15}N hPRLR-D2 in 10% (v/v) D_2O, 10 mM NaH_2PO_4, 10 mM TCEP, 1 mM DSS, and 0.02% (v/v) NaN_3 (pH 7.4) at 25°C.

(C) Overlay of [^{15}N,^{1}H]-HSQC spectra of ^{15}N hPRLR-D2 and [^{15}N,^{1}H]-TROSY-HSQC of ^{2}H, ^{15}N hPRLR-ECD shown with black and red peaks, respectively. See also Figure S1.

Not much is known about the molecular details of receptor activation, mainly because no structure of the receptor in the unbound state is available. Elegant alanine-insertion studies in the growth hormone receptor (GHR) have indicated that hormone binding most likely forces a translation of one of the transmembrane helices leading to a rotation of the ICDs and activation of the JAK2 kinases (Brown et al., 2005). Similar experiments recently ruled out a corresponding mechanism for PRLR and hence the manner in which the signal is transduced remains obscure (Liu and Brooks, 2011).

The D2 domain of PRLR contains an interesting structural feature, namely a highly conserved Trp-Ser-Xaa-Trp-Ser motif (Xaa is any amino acid), here referred to as the WS motif. This motif—or conservative variations thereof—is observed in all cytokine receptors. In the bound state of rat PRLR (rPRLR) (Broutin et al., 2010), the two Trp side chains are stabilized by strong π-cation stacking with Arg side chains, forming a structural motif that we have designated as the Trp/Arg ladder. The WS motif, and indeed the entire Trp/Arg ladder, is positioned opposite the PRL binding loop and the receptor dimerization interface. However, mutations of the WS motif to all-alanine in rPRLR decreased binding affinity for ovine PRL 23-fold (Rozakis-Adcock and Kelly, 1992). An exhaustive mutation study of 19 individual single amino acid substitutions of each of the five residues of the WS motif in the erythropoietin receptor (EPOR) revealed an extremely limited tolerance toward changes (Hilton et al., 1996). Furthermore, roles for the WS motif in receptor folding, membrane trafficking, and binding were suggested (Yoshimura et al., 1992). The residues most sensitive to changes were Trp232 and Trp235, corresponding to the human PRLR (hPRLR) residues Trp191 and Trp194 (Hilton et al., 1996; Yoshimura et al., 1992). By analogy, humans (and chickens) homozygous for a GHR mutant with the second Ser of the WS motif substituted for Leu suffer from Laron dwarfism syndrome (Duriez et al., 1993; Jorge et al., 2004), a condition which cannot be reversed by the administration of GH. Free-energy perturbation calculations on the interleukin-4 receptor suggested a role for the WS motif as a gatekeeper, ensuring a nonactive state via interactions with the lipid membrane (Weidemann et al., 2007). So far, however, a general role in receptor triggering is lacking.

We have characterized the extracellular domain of the hPRLR and present, to our knowledge, the first structural description of the hPRLR *off-state.* In atomic detail, the WS motif acts as a molecular switch controlling whether the receptor is in the *off-state* or in the *on-state*. Our results indicate an allosteric communication line from the hormone binding site via the WS motif and extracellular dimerization site 3 to the membrane-proximal pole of the receptor.

RESULTS

Initially, the solution structure of unbound hPRLR-ECD was pursued. Even with per-deuterated protein, a significant lack of

signals was evident in the [^{1}H,^{15}N]-transverse relaxation optimized spectroscopy (TROSY)-heteronuclear single quantum coherence (HSQC) spectrum. More critically, the triple-resonance heteronuclear nuclear magnetic resonance (NMR) spectra were of poor quality, impairing sequential assignment of chemical shifts and suggested undesired conformational dynamics, aggregation, or oligomerization of hPRLR-ECD under the conditions of the NMR experiment. Hence, the two domains of hPRLR-ECD were expressed individually.

The [^{1}H,^{15}N]-HSQC spectrum of hPRLR-D1 revealed this to be responsible for the lack of signals in the spectra of hPRLR-ECD (Figure S1 available online). hPRLR-D2 gave instead rise to a [^{1}H,^{15}N]-HSQC spectrum with the expected number of signals and a dispersion indicating a folded domain in the absence of hPRLR-D1 (Figure 1B). When overlaid with the [^{1}H,^{15}N]-TROSY-HSQC spectrum of ^{2}H^{15}N-hPRLR-ECD, most signals were readily superimposable (Figure 1C), suggesting the structure of isolated hPRLR-D2 to closely resemble that in hPRLR-ECD.

Structure of the Unbound hPRLR-D2 and Differences Between Unbound and PRL-Bound Receptor

Assignments of resonances in hPRLR-D2 resulted in a completeness of 92.8% in all backbone and side chain resonances, and the final structure set yielded the statistics shown in Table S1A. A stereo image of the backbone ribbon of the ensemble and a ribbon representation of the structure is shown in Figures 2A and 2B. Seven β strands (A–G) are present forming two antiparallel β sheets (Figure 2C). One sheet contains three short strands (A, Leu107-Lys114; B, Tyr122-Ser128; E, Glu166-Ile169) and the other consists of four strands with strand F extended compared to the others (C, Tyr144-Pro150; D, Glu157-Gly162; F, Lys177-Cys184; G, Thr198-Ile202). The structure of the unbound hPRLR-D2 represents an FNIII fold.

To our knowledge, the structure of hPRLR-D2 provides the first insight into the unbound state of PRLR. Compared to published structures of full-length PRLR-ECD with PRL bound, our current hPRLR-D2 structure has an overall similar fold to the D2 domain in bound hPRLR-ECD with C$^{\alpha}$ root mean square deviations ranging from 1.2 Å to 1.7 Å (Table S1B). Striking local differences were observed between the free and the PRL-bound states, especially in the composition of the two sheets (Figure 3A). Compared to the bound state of the hPRLR-ECD, the C and F strands were prominently shorter in hPRLR-D2, and the A and B strands were slightly longer.

Pronounced conformational differences in the conserved WS motif in which all PRLR-ECD complex structures have a structured Trp/Arg ladder were observed (Figure 3B). Such an arrangement is only partly formed in unbound hPRLR-D2. The lower part of the ladder consisting of Lys149-Trp156-Arg147-Trp194 was formed, whereas the upper part of the ladder involving the indole rings of Trp191 and Trp194 of the WS-motif were observed in an edge-to-face arrangement (Figure 3C). The proton resonances from the side chain of Arg183 involved in stacking with the Trp side chains in the bound state were absent in the total correlation spectroscopy (TOCSY) and nuclear Overhauser enhancement spectroscopy (NOESY) spectra. By contrast, the formation of the lower part of the Trp/Arg ladder was supported by distinct NOEs.

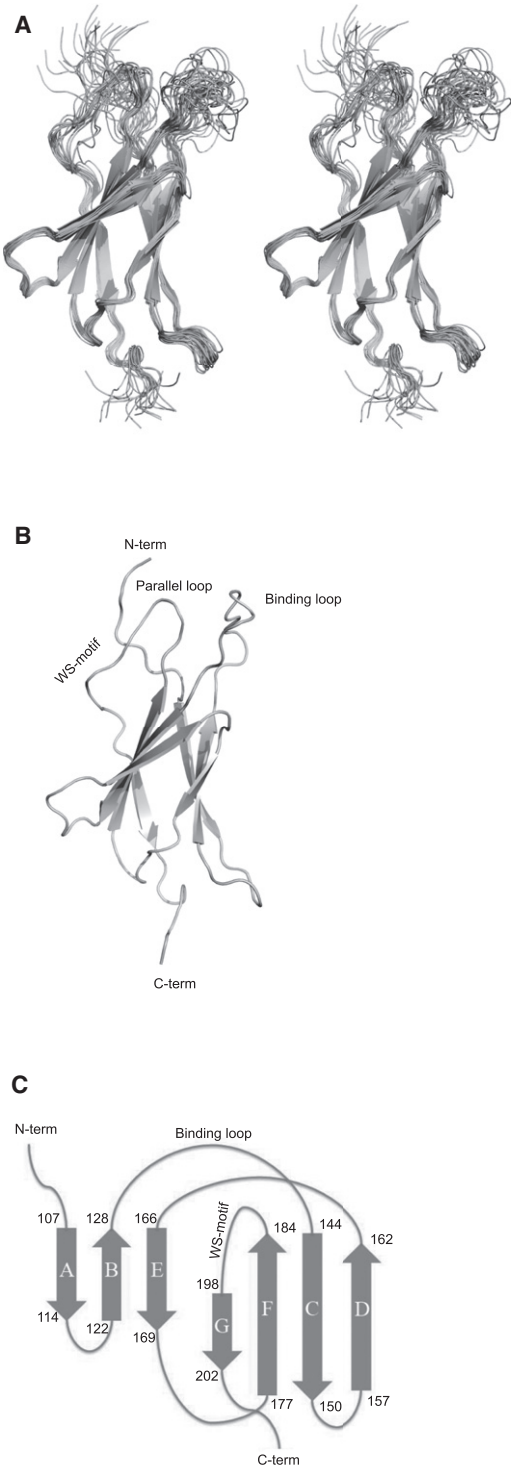

Figure 2. NMR Solution Structure Ensemble of hPRLR-D2

(A) Stereo view (cross-eyed) of the 10 lowest energy structures aligned using backbone atoms of the seven β strands, root mean square deviations of 0.4 ± 0.1 Å.

(B) Schematic representation of the lowest energy structure of hPRLR-D2.

(C) Topology representation of hPRLR-D2. Arrows indicate the directions of the β strands A–G. The N-terminal, C-terminal, binding loop, and WS motif are labeled. The β strands are indicated by residue numbers.

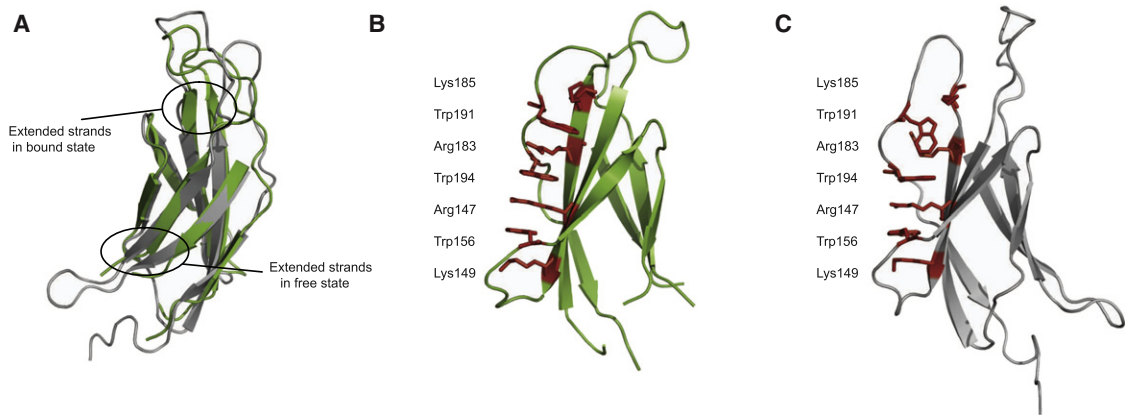

Figure 3. Comparison of Free and Bound States of hPRLR-D2

(A) Overlay of hPRLR-D2 (gray) with the structure of D2 from hPRLR-ECD (green) extracted from the 1:1 bound state (Protein Data Bank ID:3D48). The two structures were aligned by PyMOL; for clarity, residues prior to 107 are not shown in hPRLR-D2.

(B) Structure of bound hPRLR-D2 (Protein Data Bank ID:3D48). The Trp/Arg ladder residues Lys149, Trp156, Arg147, Trp194, Arg183, Trp191, and Lys185 are shown in red.

(C) Structure of unbound hPRLR-D2 with hydrogen atoms omitted. The T-stack of Trp191 and Trp194 and the remaining side chains participating in Trp/Arg ladder in the bound state are displayed in red.

The T-Stack Is a Structural Feature of the Unbound State

The existence of two different structural states of the receptor, one adopting a Trp/Arg ladder conformation in the bound state (Figure 3B) and the other an edge-to-face conformation in the unbound state (Figure 3C), was supported by circular dichroism (CD) analysis. An edge-to-face orientation of the indole rings of Trp gives rise to a characteristic positive ellipticity from π-π^* exciton-coupling around 230 nm (Wu et al., 2009). Intense positive ellipticities at 230 nm for hPRLR-ECD and 228 nm for hPRLR-D2 and a broad band at 210-213 nm were observed (Figure 4A). The edge-to-face conformation is termed a T-stack. In the structure of unbound hPRLR-D2, T-stacking was observed for Trp191 and Trp194. Although the present NOE set was not sufficient to orient the T-stack optimally (see below), no other aromatic rings in hPRLR-D2 appeared to engage in such an arrangement.

To support the conclusion of a T-stack in the unbound state of hPRLR-D2, we selectively labeled the C^{δ} of Phe and Tyr, $C^{\delta 2}$ and $C^{\varepsilon 1}$ of His, and $C^{\delta 1}$ and $C^{\varepsilon 3}$ of Trp using $^{13}C_1$-glucose (Teilum et al., 2006) and recorded a [^{1}H,^{13}C]-TROSY-HSQC. Especially for Trp side chains, the only protons that would be connected to a ^{13}C-labeled carbon using this selective labeling approach would be $H^{\varepsilon 3}$ protons. If a T-stack was present in hPRLR-D2, this would give rise to a significantly up-field shifted $H^{\varepsilon 3}$ of the edge Trp (Andersen et al., 2006) in this case of Trp191. We observed a peak at 5.1 ppm/132 ppm diagnostic of a T-stack (Figure 4B). Recursively, from the NOESY spectra, this peak was assigned to $H^{\varepsilon 3}$ of Trp191, confirming the presence of the T-stack between Trp191 and Trp194 (Figure 4C). The aromatic rings of Trp191 and Trp194 in the final structure of hPRLR-D2 seem too far apart to what is suggested from the ring current shifts, and it appears that the present set of NOEs is not adequate in defining the orientation of the rings precisely. Thus, dynamics as manifest in intermediate exchange in the ^{15}N dimension, where the peak is broad, supporting a possible exchange process (Figure 4B).

Finally, we investigated whether the T-stack in hPRLR-ECD also implicated Trp191 and Trp194. Although the NMR spectrum also contained peaks from hPRLR-D1, the superimposition of peaks from hPRLR-D2 made the transfer of assignments in the Trp indole region of the HSQC spectrum straightforward. A comparison of the NMR signals from the indole NH protons of hPRLR-ECD and -D2 in their unbound states showed that the chemical environment around these are likely similar, supporting the presence of the T-stack in hPRLR-ECD (Figure 4D).

The T-Stack Rearranges to Form the Trp/Arg-Ladder by PRL Binding

The structures of the PRL-bound state of PRLR-ECD suggested that the T-stack of the unbound state rearranges to form the Trp/Arg ladder in the bound state. The Trp exciton coupling was used to follow hormone binding by comparing the far-UV CD spectra of unbound and hPRL-bound hPRLR-ECD (Figure 4A). This was done by subtracting the CD spectrum of the sum of the spectra of PRL and hPRLR-ECD from that of the spectrum of the hPRL:hPRLR-ECD complex. A significant loss in signal intensity was seen at 228 nm. A loss of the Trp-Trp π-π^* exciton coupling upon PRL binding would expectedly lead to a concomitant loss of an opposite signed feature at 216 nm, which is not observed here. However, because formation of the complex between PRLR-ECD and PRL leads to increased β-sheet and α-helix stabilization, this will mask the signature at 216 nm. Thus, it appears that PRL binding to PRLR-ECD leads to a conformational change involving the WS motif as suggested from the structures.

Titration of ^{15}N-labeled hPRLR-D2 with unlabeled hPRL resulted in the chemical shift changes shown in Figure 5B. Although small, these were reproducible, as similar results from three individually prepared samples were obtained. The chemical shift changes in hPRLR-D2 were spread throughout the domain, with minimal changes in the β strands. The largest chemical shift changes were observed in the binding loop

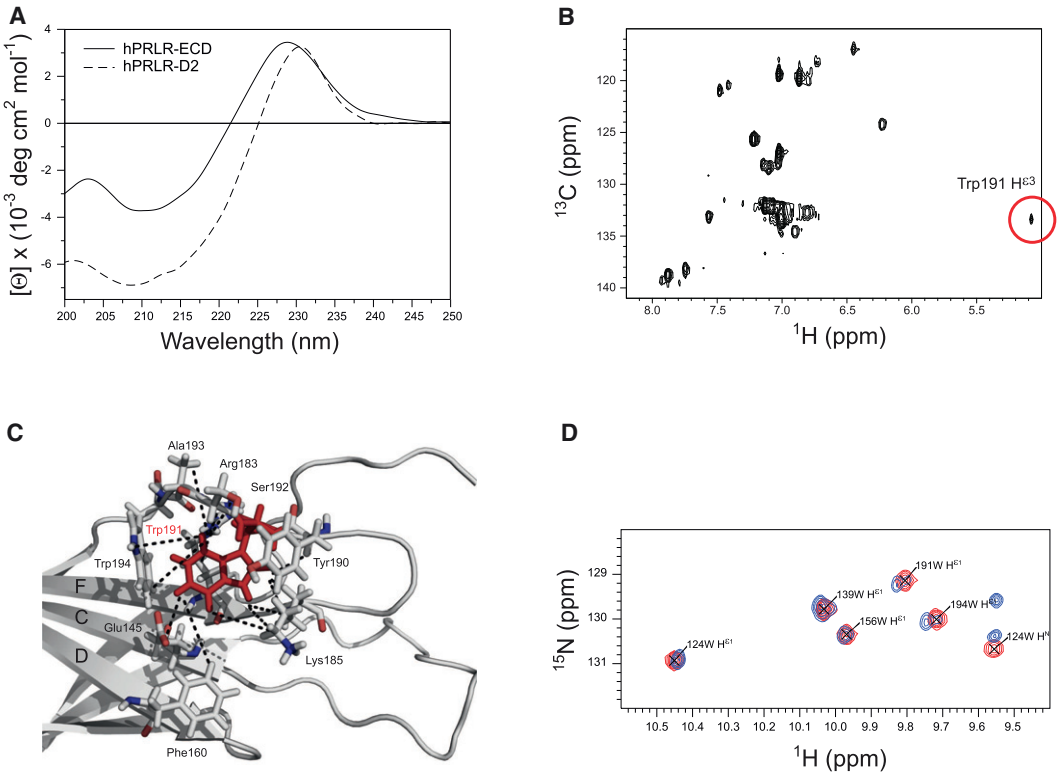

Figure 4. The WS Motif in hPRLR-D2 and ECD Adopts a T-Stack Conformation in the Unbound State

(A) Far-UV CD spectra of free hPRLR-D2 (dashed) and free hPRLR-ECD (solid) recorded on 5 μM protein samples in 10 mM Na_2HPO_4 (pH 7.4).

(B) Aromatic [^{13}C,^{1}H] TROSY-HSQC spectrum of $^{13}C_1$-labeled hPRLR-D2. The peak at 134/5.1 ppm (red circle) stems from Trp191 $H^{\varepsilon 3}$ and is indicative of an edge-to-face Trp-Trp stacking.

(C) The NOEs involving indole resonances of Trp191 shown on the hPRLR-D2 structure. Trp191 is shown in red, with NOEs indicated by dashed lines and contact residues labeled and shown as sticks.

(D) Overlay of the Trp indole region of hPRLR-D2 and hPRLR-ECD [^{15}N,^{1}H]-HSQC spectra in red and blue, respectively. The full spectra are shown in Figure 2B. The additional blue peak at 129.5/9.55 ppm is from the hPRLR-D1.

(residues 132–133 and 138–141), the N terminus (residues 100–102), the parallel loop adjacent to the conserved WS motif (residues 188–195) and the loop between β strands A and B (AB loop; residues 117–120) (Figure 5C). The chemical shift changes observed for the binding loop are in accordance with recently published structures (Broutin et al., 2010; Svensson et al., 2008; van Agthoven et al., 2010) and were corroborated by corresponding shifts in binding site 1 of ^{15}N-hPRL when titrated with hPRLR-D2 (Figure S2). The chemical shift changes in the conserved WS motif of hPRLR-D2, which is located opposite the binding interface, as well as in the AB loop most distant from the binding loop, were more surprising. The AB loop exhibited chemical shift changes of the same magnitude as those of the binding loop. Thus, the binding of hPRL disseminates from the binding pole of hPRLR-D2 to the membrane proximal pole.

Nine additional residues positioned more than 5 Å from any binding site residue were affected by hPRL binding. Five of these—Ile146, Glu151, Glu155, Tyr178, and Arg183—are evolutionarily conserved. The chemical shift changes observed for Tyr178 and Lys185, both of the F strand, were presumably due to the β-strand extensions observed in structures of hormone-bound PRLR. Residues Glu151, Lys152, and Glu155 are all located in the CD loop, and the changes observed for these residues could be a direct effect of the changes observed for Tyr178 through van der Waals interactions. Finally, Phe206 is close to the AB loop.

A similar approach was taken to analyze PRL-induced chemical shift changes in hPRLR-ECD. This was hampered by large shifts and the aforementioned difficulty of obtaining triple-resonance spectra for assignment. As an alternative, we focused on the region of the indole NH resonances of hPRLR-ECD (Figure 5D). Here, the assignments from D2 were readily transferable, and only two peaks were observed to change in response to PRL binding. These were Trp139 from the binding loop and Trp191 rearranging the T-stack to the Trp/Arg ladder.

Impact on Site 3 Residues by the Constitutively Active hPRLR^{I146L} Mutation

The constitutively active receptor-variant hPRLR^{I146L} was anticipated, at least in part, to be able to assume the active conformation of the receptor in the absence of ligand. Because of the partial constitutive activity observed for the I146L-variant, it might provide information relating to the bound state of the hPRLR as well as to the activation process. This prompted a comparative study of hPRLR^{I146L} versus wild-type.

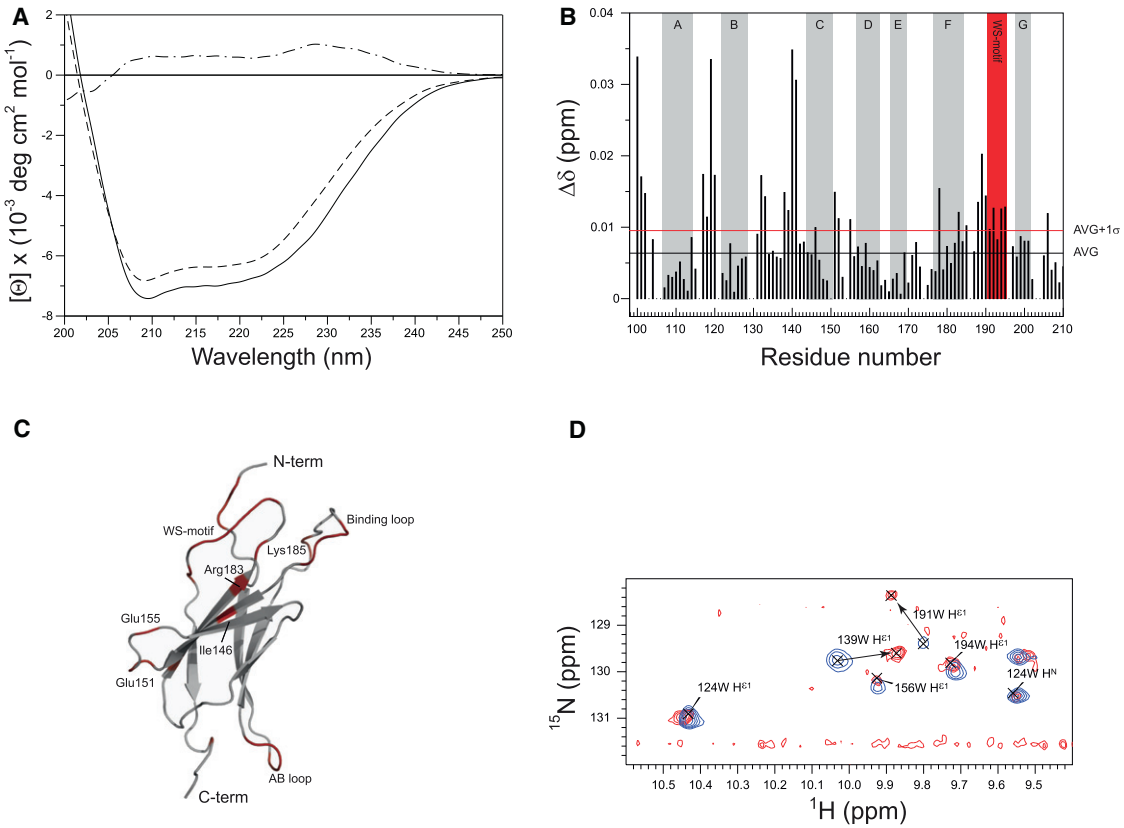

Figure 5. Titration Experiments of hPRL with hPRLR-D2 and ECD

(A) Far-UV CD spectra of the 1:1 hPRLR-ECD:hPRL complex (solid line), sum of the spectra of hPRLR and hPRLR-ECD (dashed line), and the difference spectrum of complex and sum highlighting the structural changes by complex formation (dashed/dotted line).

(B) Chemical shift perturbations of hPRLR-D2 titrated with hPRL. The weighted average and average plus 1 SD are marked by a horizontal black and red line. Secondary structures are indicated by gray bars, and the WS motif is indicated by a red bar.

(C) hPRLR-D2 residues with Δδ above 1 SD from the average are shown in red on hPRLR-D2.

(D) Spectra of ^{2}H, ^{15}N-hPRLR-ECD with (red) and without (blue) hPRL present in a 1:2 molar ratio. The Trp indole region of the [^{15}N,^{1}H]-TROSY-HSQC spectra is shown, with Trp139 of the binding loop and Trp191 of the WS motif experiencing the largest changes (arrows).

See also Figure S2.

Attempts to obtain hPRLR-ECD^{I146L} by refolding were unsuccessful. The same mutation was therefore introduced into hPRLR-D2, producing a folded hPRLR-D2^{I146L}. Importantly, the positive ellipticity at 228 nm seen in unbound hPRLR-D2 and hPRLR-ECD (Figure S3) was retained, suggesting a complementary origin for the associated constitutive activity. We compared the backbone N-H^{N} chemical shifts of hPRLR-D2 and hPRLR-D2^{I146L} (Figure 6A). The largest chemical shift changes were observed for residues within a distance of 5 Å from the mutation site and were attributed to local chemical changes introduced by the mutation. Two groups of residues further than 5 Å from the mutation site also showed significant chemical shift changes. The first group of Gly162-Gln164, Lys168, Ser171 and His173 (Figure 6B) are all located in the site 3/receptor-dimerization interface. The second group of Ala110, Val111, and Glu112 in the A strand and Tyr122, Leu123, and Ser128 in the B strand are located in the strands restructuring upon dimerization. Finally, changes were observed for Thr198 and Phe199, which interact closely with the affected A strand Val111.

Altered Dimerization Potential of hPRLR-D2^{I146L} as the Origin of Constitutive Activity

Global and local dynamic properties of hPRLR-D2 and hPRLR-D2^{I146L} were assessed from NMR relaxation measurements of backbone ^{15}N spins (Figure 7). The ratio between the transversal relaxation rate, R_2, and the longitudinal relaxation rate, R_1, for residues in structured parts of the polypeptide chain represents an estimate of the overall rotational correlation time, τ_C, of the protein. Residues in flexible regions such as loops with internal dynamics faster than τ_C will have R_1 values higher than average and R_2 values lower than average, and vice versa for dynamics slower than τ_C.

For the wild-type, the relaxation data are typical for a stable protein of around 100 residues. The relaxation rates are fairly similar for the residues in the β strands, which are assumed to be the most rigid parts of the protein. The binding loop (Asp134-Leu143), the parallel loop (Asp187-Gly189), and the C- and N-terminal regions have R_1 values significantly above and R_2 values significantly below the averages, indicating dynamics faster than the overall rotational diffusion of the molecule.

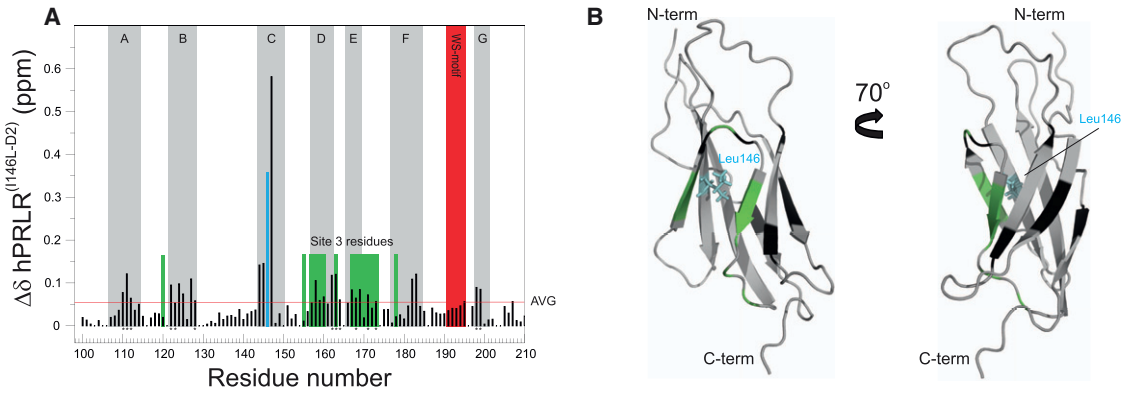

Figure 6. Comparison of the Chemical Shift of hPRLR-D2 and hPRLR-D2^{I146L}

(A) Backbone amide chemical shift differences ($\Delta\delta = ((\Delta\delta_H)^2 + (0.25*\Delta\delta_N)^2)^{0.5}$) between free hPRLR-D2 and the free hPRLR-D2^{I146L} (spaces represent proline residues). The weighted average is marked by a horizontal red line. Positions of the β strands are indicated by gray bars, and the WS motif is indicated as a red bar. Asterisks indicate residues with significant chemical shift changes that are located more than 5 Å from the mutation site. Green bars indicate residues with site 3 interactions in the bound state.

(B) Residues with Δδ above average and positioned more than 5 Å from the mutation site. In green residues of site 3 and in black residues outside site 3, Ile146 is shown as cyan sticks. The structure is rotated to illustrate both sides of the β sandwich.

See also Figure S3.

From the relaxation data, τ_C was estimated to 9.9 ns for hPRLR-D2 by the program Tensor2 (Dosset et al., 2000). For a few residues, and most distinctly for Glu108, Arg183, and Trp194, R_2 is slightly elevated, which may be an indication of conformational exchange on the milli- to microsecond time scale (Figure 7A).

The relaxation data from the hPRLR-D2^{I146L} mutant showed two distinct differences as compared to the wild-type data. First, there is a general increase in R_2. Consequently, the average R_2, $\langle R_2 \rangle$ = 21.7 ± 0.8 s^{-1} and $\langle R_2/R_1 \rangle$ = 19.2 ± 1.5 are significantly higher than for wild-type where $\langle R_2 \rangle$ = 15.7 ± 0.7 s^{-1} and $\langle R_2/R_1 \rangle$ = 13.8 ± 1.2. This difference suggests an increase in τ_C, which is estimated to 11.7 ns for hPRLR-D2^{I146L}. This may be explained by transient dimerization. If we, as a first approximation, assume spherical geometry of both the monomer and the dimer, full dimerization will result in doubling of τ_C. The increase in τ_C, from 9.9 ns to 11.7 ns, thus corresponds to hPRLR-D2^{I146L} being 18% dimeric. Second, for more residues than seen in the wild-type, R_2 is increased above the average and the increase is larger. Specifically, the increase is most pronounced for residues in the N terminus and for residues in the WS motif (Figures 7A and 7D). Taken together, the relaxation data suggest that hPRLR-D2^{I146L} undergoes fast, transient dimerization and slow conformational exchange in the WS motif.

To explore the possibility of a dimeric state of hPRLR-D2^{I146L}, the hydrodynamic radius was determined by NMR diffusion experiments, as well as by small-angle X-ray scattering (SAXS) analysis (Table 1). Here, it was evident that the two proteins exhibited similar hydrodynamic radii, R_H, of around 22 Å in solution. The measured radii are in close agreement with the theoretical hydrodynamic radius of 23 Å calculated with HYDROPRO for a monomer using the hPRLR-D2 solution structure. Thus, hPRLR-D2 and hPRLR-D2^{I146L} both exist predominantly as monomers in solution. However, the resolution of the two methods does not allow the detection of a low populated dimer state (<20%), which could discriminate the two receptor variants.

To rule out the possibility that the differences in relaxation rates between hPRLR-D2 and hPRLR-D2^{I146L} could be due to a global destabilization and unfolding, their global stability, $\Delta G^{H2O}{}_{N\text{-}D}$, against chemical denaturation were determined by intrinsic fluorescence (Figure 8). The I146L mutation caused no significant destabilization of hPRLR-D2 within one standard deviation with $\Delta G^{H2O}{}_{N\text{-}D}$ of −41 ± 3 kJ mol^{-1} (hPRLR-D2) and −38 ± 5 kJ mol^{-1} (hPRLR-D2^{I146L}).

DISCUSSION

To our knowledge, our structural characterization of the PRLR provides for the first time insight into the role of the conserved WS motif in cytokine receptor activation. The hPRLR-D2 solution structure revealed structural differences by comparison to structures of the D2 domain of hormone-bound receptors (1F6F, 3EW3, 3D48, 3MZG, and 3NPZ) and other members of this cytokine receptor family, such as EPOR (1EER) and GHR (2AEW). The differences consistently mapped to the WS motif and to the lengths of the β strands constituting the two sheets characteristic of the FNIII domain. In the unbound hPRLR-D2, an edge-to-face orientation forming a T-stack of Trp191 and Trp194 from the WS motif was observed via a highly upfield shifted $H^{\varepsilon 3}$ resonance of Trp191 and supported by a characteristic aromatic exciton coupling measured by far-UV CD spectroscopy. The T-stack also exists in the full hPRLR-ECD, which indicates a specific role for this structure.

The description of the T-stack orientation of the WS motif in PRLR is unprecedented in any cytokine receptor. Crystal structures of the EPOR and the GHR have been published in the free (1ERN and 2AEW) and bound states (1EER and 1A22). These reveal that the cytokine binding sites of two adjacent molecules of the free form interact to form a large crystal-packing interface (~1700 $Å^2$), matched by a similar 960 $Å^2$ crystal-packing interaction in GHR. In all states of EPOR and GHR, the WS motif adopts the ladder conformation. However, CD spectra of their free forms

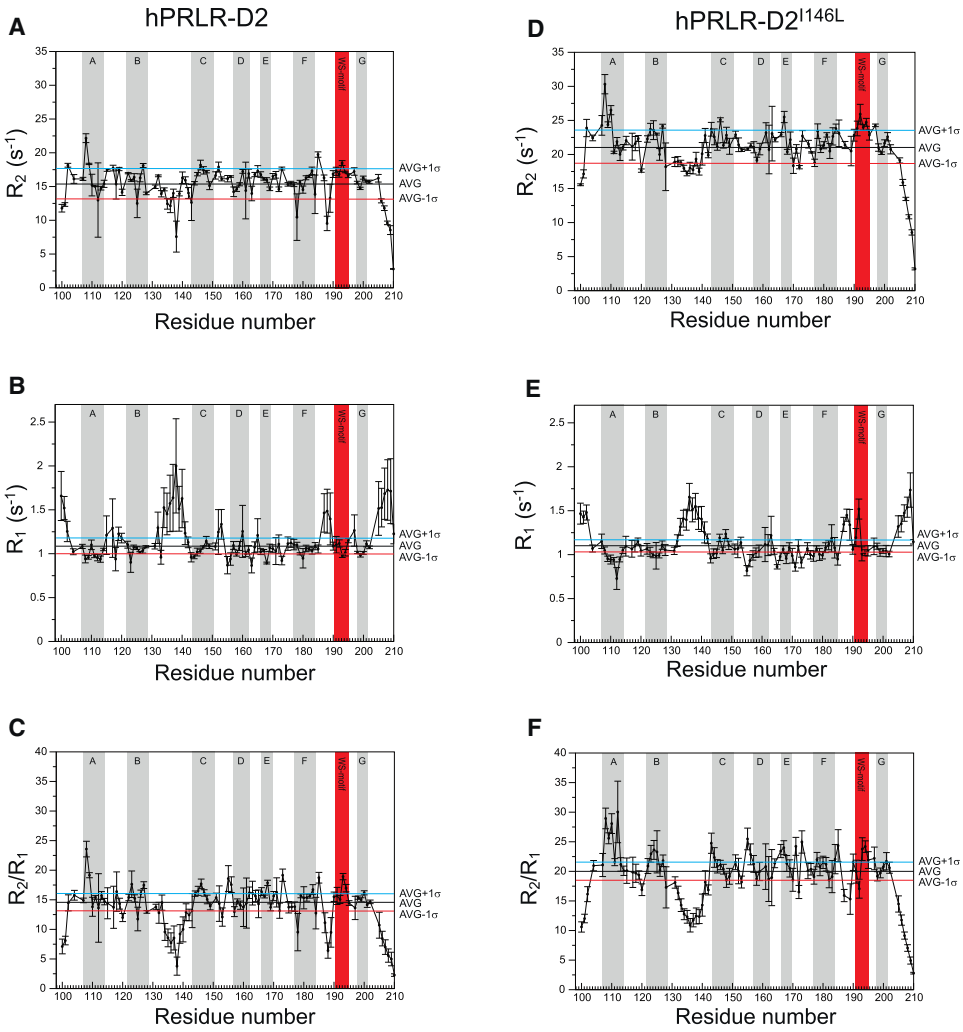

Figure 7. Relaxation Properties of hPRLR-D2 and hPRLR-D2^{I146L}

(A and D) Transverse relaxation rate constants, R_2. The trimmed averages are: hPRLR-D2, $< R_2 > = 15.7 \pm 0.7\ s^{-1}$ and hPRLR-D2^{I146L}, $< R_2 > = 21.7 \pm 0.8\ s^{-1}$. (B and E) Longitudinal relaxation rate constants, R_1. The trimmed averages are: hPRLR-D2, $< R_1 > = 1.08 \pm 0.07\ s^{-1}$ and hPRLR-D2^{I146L}, $< R_1 > = 1.1 \pm 0.07\ s^{-1}$. (C and F) R_2/R_1 ratios. The trimmed averages are $< R_2/R_1 > = 13.8 \pm 1.2$ for hPRLR-D2 and $< R_2/R_1 > = 19.2 \pm 1.5$ for hPRLR-D2^{I146L}. All parameters are shown as a function of the residue number, and the trimmed averages are marked by horizontal lines. Positions of the β strands are indicated by gray bars and the WS motif is indicated by a red bar. Missing data points are due to overlap and/or proline residues. Error bars represent the SE from fits of the experimental data.

reveal positive ellipticity around 228 nm, suggesting that they adopt the T-stack conformation in solution. Despite sequence differences between the WS motif of hGHR (Bass et al., 1991) and hPRLR, a positive edge-to-face 228 nm band is present but less pronounced for hGHR. The CD spectra of unbound EPOR (Narhi et al., 1997) and of unbound hPRLR are strikingly similar. Both receptors have the characteristic positive aromatic exciton coupling at 228 nm and the broad negative band at 210–213 nm, arguing for an aromatic contribution to the far-UV CD and the presence of a T-stack in both structures. The first Trp in the WS motif is the one that in the free state stacks edge-on with the second Trp. The latter has the same orientation in both states. In the two crystal structures of the free receptors, the first residue (Trp209 in EPOR, Tyr222 in GHR) has higher B factors than the second one (Trp212 in EPOR, Phe225 in GHR). In the complex structures, the B factors are the same. We propose this reflects the fact that although the Trp/Arg ladder is formed in the crystal without the cytokine, it does not reach the local energy minimum of the cytokine-induced *on-state*.

There are presently five other solution structures of unbound cytokine receptors with a WS motif available; the human interleukin-6 receptor (IL6R) (Hecht et al., 2006), the cytokine-binding-domain of the common β chain of the receptor for granulocyte macrophage colony-stimulating factor (D4β_c) (Mulhern et al., 2000), the granulocyte colony stimulating factor receptor (Yamasaki et al., 1997), the signal transducer gp130 (Kernebeck et al., 1999), and the C-terminal domain of the ciliary neurotrophic factor receptor (CNTFR) (Man et al., 2003). In all but D4β_c and CNTFR, there are missing assignments for Trp/Arg ladder residues. Nonetheless, the Trp/Arg ladder is present in those structures, suggesting that the formation is dictated by force fields and not by experimental observation. However, when

Table 1. Measured and Theoretically Estimated Hydrodynamic Radii of hPRLR-D2 and hPRLR-D2^{I146L}

Hydrodynamic Radius (R_H)	hPRLR-D2	hPRLR-D2^{I146L}
PSG-LED (Å)	22.32	20.49
SAXS (Å) R_H (R_g)	25.5 (19.7 ± 0.03)	22.8 (17.6 ± 0.2)
HYDRO-PRO (Å)	23	23

Hydrodynamic radius was calculated from the Protein Data Bank file as described (García De La Torre et al., 2000).

assignments of Trp/Arg ladder residues have been completed, the T-stack is either partly formed as in IL6R, or when a shifted Trp $H^{\varepsilon 3}$ resonance has also been assigned, a stabilized T-stack is observed as in CNTFR. Moreover, in the CD spectrum of IL6R, the aromatic exciton coupling is present (Ozbek et al., 1998), supporting T-stack conformation. Thus, the T-stack may be a general trait of unbound cytokine receptors harboring the WS motif.

The WS Motif Acts as a Hormone-Dependent Molecular Switch

The reorganization of the WS motif leading to formation of the Trp/Arg-ladder upon receptor activation could be hypothesized to be allosterically controlled and initialized by hormone binding. Key residues in PRL binding are Trp139 of the binding loop and His188 of the parallel loop. The latter is directly connected to the WS motif. Although modest, PRL binding led to reproducible and significant changes in chemical shifts of residues in the binding loop, the parallel loop, the AB loop, and the N-terminal and of residues involved in the Trp/Arg ladder (Arg183 and Trp194). PRL induced restructuring of the T-stack by CD for hPRLR-ECD, but not for hPRLR-D2. Moreover, titration of hPRLR-ECD with PRL pinpointed Trp191 with the largest observed chemical shift change, even though it has no contact with PRL. This underlines that hormone binding to hPRLR induces a conformational switch in the WS motif and suggests that conformational change plays a role in receptor activation. The generality of the conformational change from the T-stack to the Trp/Arg ladder is supported by similar reported loss of the aromatic exciton upon EPO binding to the EPOR-ECD (Narhi et al., 1997), analogous to what we observed for the hPRLR-ECD. Together with the presence of a Trp/Arg ladder in all bound states of cytokine receptors, this suggests a commonly observed *on-state* conformation by the Trp/Arg ladder.

The structural differences between unbound and hormone-bound hPRLR-D2 pinpointed here, combined with our additional NMR data and spectroscopic data from other cytokine receptors, imply a significant role for the two tryptophans of the WS motif in keeping the unbound receptor in an inactive state. T-stacks have been shown to stabilize hairpins by ~5 kJ mol^{-1} (Andersen et al., 2006). Thus, such a conformation in hPRLR most likely provides a significant energetic contribution to hPRLR *off-state* stabilization. Several mutations of residues in WS motifs have been performed, showing effects on folding, binding, and expression levels (Baumgartner et al., 1994; Hilton et al., 1996; Rozakis-Adcock and Kelly, 1992). Mutation introduced outside the motif however, could in principle stabilize or destabilize either conformation, leading to either enhanced or decreased affinity for the hormone. This conundrum is so far unresolved.

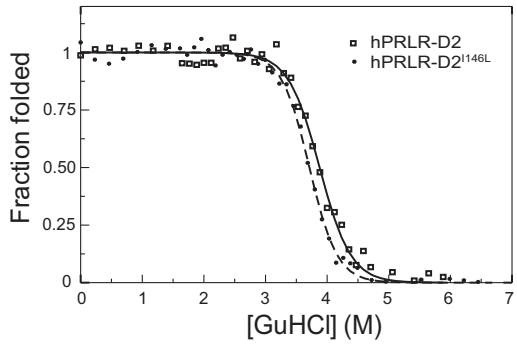

Figure 8. Chemical Denaturation of hPRLR-D2 and hPRLR-D2^{I146L} Followed by Intrinsic Fluorescence

The normalized two-state GuHCl denaturation curves of the hPRLR-D2 (□) and hPRLR-D2^{I146L} (●) measured from emission at 342 nm at 25°C with excitation at 280 nm; the solid line indicates fits to two-state unfolding. Sample conditions were 50 mM Na_2HPO_4, 10 mM TCEP (pH 7.4), and 5 μM protein.

Additional support for a role of D2 in restraining the free receptor in the *off-state* comes from deletion mutations performed in rabbit (Gourdou et al., 1996) and in human (Tan et al., 2008) PRLR. Cell-expressed D2-deleted receptors exhibited ligand-independent activation of transcription in vitro, suggesting a negative regulatory effect of D2 in hPRLR. A similar deletion of D1 did not lead to constitutive activation but lowered hormone affinity by three orders of magnitude and shifted the activation profile to higher hormone concentration (Gourdou et al., 1996; Kline et al., 2002). It was suggested that D2 is responsible for a specific negative effect on signal transduction. This negative effect, we suggest, is encoded in the WS motif established in D2 to stabilize the *off-state* acting as a molecular switch turned on by hormone binding.

Transient Dimers in the Constitutive Active Receptor Variant

The analyses of relaxation and chemical shift changes between hPRLR-D2^{I146L} and wild-type (wt)-hPRLR-D2 mapped distinctly to the site 3 residues as well as to the WS motif. The I146L point mutation furthermore led to a redistribution of the dynamics of the fibronectin core (Figure 7), leading to transient dimerization detected by a decreased tumbling rate of the mutant protein. Taken together with the constitutive activity measured for full-length hPRLR^{I146L} in cells, this finding suggests that a low-lying excited state representing the *on-state* of the receptor in the absence of the hormone is sampled more often than in wt-hPRLR. That the T-stack, which stabilizes the *off-state*, is still formed in hPRLR-D2^{I146L} implies that hPRLR^{I146L} should not be fully active. This agrees with the submaximal activity measured for the non-PRL-stimulated hPRLR^{I146L} variant. Thus, only when the Trp/Arg ladder and D2-D2 interface are formed will the receptor be fully active. In further support of this suggestion, it was found that the affinity for the hormone in stably transfected HEK293 clones was identical for both receptors, but the efficacy was higher for the constitutively active variant (Bogorad et al., 2008; Courtillot et al., 2010).

The WS Motif Links Hormone Binding to the Dimer Interface

The present study has provided insight into the *off-state* of the PRLR receptor and into the path from the *off-state* to the activated *on-state*. Activation of PRLR involves allosteric modulation of the WS motif, which contributes to the stability of the *off-state* by an edge-to-face T-stack of the Trp191 and Trp194 indole rings. When the hormone interacts with the binding and parallel loops, a conformational response is transmitted to create the Trp/Arg ladder, mature the dimerization interface, and perturb the AB loop. The results support the hypothesis that binding of the first receptor is mandatory for forming a trimeric signaling complex (Broutin et al., 2010), making sequential receptor binding compulsory. Although the receptors may be predimerized on the cell surface (Gadd and Clevenger, 2006; Tallet et al., 2011), they must be organized such that molecular switches will assure the stability of the *off-state*. One such switch, the T-stack, has been described here. The present elucidation of an allosteric communication line from the hormone binding site via the WS motif and the receptor site 3 to the membrane-anchored pole of the receptor may represent the mechanism by which hormone binding is transmitted to the membrane. By analogy, the switch mechanism and signal transduction network may be general features of membrane-bound cytokine receptors. A detailed understanding of these mechanisms will open novel routes to the continued optimization of receptor antagonists.

EXPERIMENTAL PROCEDURES

Plasmids for Expression of the D1 and D2 Domains (NM_000949)

Recombinant hPRLR-D2$^{99–210}$ and hPRLR-D1$^{1–102}$ were amplified from IRAKp961G13133Q (RZPD German Resource Center for Genome Research) (primers in supplemental data), purified using the Wizards-plus-SV miniPrep DNA (Promega, Madison, WI), and sequences were confirmed (MWG biotech, Ebersberg, Germany).

Protein Expression and Purification

The hPRLR-D2 expression from *E. coli* BL21(DE3), either labeled or unlabeled (Teilum et al., 2005), was induced with IPTG (1 mM) at $OD_{600} \approx 0.6$ for 4 hr at 37°C, and cells were sonicated to bring hPRLR-D2 in solution. After $(NH_4)_2SO_4$ precipitation, 75% (w/v), stirring for 2 hr at 0°C, the precipitate was dissolved in 30 mM NH_4HCO_3, 100 mM NaCl, and 1 mM dithiothreitol (DTT) (pH 8.0) and applied to a SephadexG50-Fine (GE Healthcare) column (24 × 370 mm, 167 ml). hPRLR-D2 fractions were pooled, concentrated, and buffer exchanged. For structure determination, the NMR sample contained 0.5 mM ^{13}C,^{15}N-hPRLR-D2 in 10% (v/v) D_2O (or 99.9% D_2O), 10 mM NaH_2PO_4, 10 mM TCEP, 1 mM DSS, and 0.02% (v/v) NaN_3 (pH 7.4). For the relaxation experiment, a MonoQ column (1 ml, GE Healthcare) was introduced to remove minor impurities, equilibrated in 20 mM Tris-HCl and 1 mM DTT (pH 9), and eluted by a linear gradient of NaCl. The hPRLR-D2^{I146L} followed the same protocol. hPRL and hPRLR-ECD were purified as described (Teilum et al., 2005); D1 followed the protocol for hPRLR-ECD. D1, hPRLR-ECD, and hPRLR-D2^{I146L} were either ^{2}H,^{15}N-labeled from M9 media grown in 99% D_2O, ^{15}N-labeled, or unlabeled from LB.

NMR Spectroscopy

Either an 800 MHz Varian INOVA spectrometer equipped with a 5 mm triple-resonance cryoprobe with a Z-field gradient, or an 800 MHz Bruker Avance spectrometer equipped with a 5 mm TCI cryoprobe was used to record the following NMR experiments at 25°C: [^{15}N,^{1}H]-HSQC, HNCO, HN(CA)CO, HN(CO)CA, HNCA, CBCA(CO)NH, HNCACB, C(CO)NH, H(CCO)NH, TOCSY ^{15}N-HSQC, HCCH-TOCSY, NOESY ^{15}N-HSQC (mix 150 ms), aromatic NOESY-^{13}C-HSQC (mixing time 100 ms), and aliphatic NOESY-^{13}C-HSQC (mix 140 ms). Assignment of aromatic side chains was aided by HBCBCHCDHD and HBCBCGCDCEHE spectra (Yamazaki et al., 1993). FIDs were processed using nmrPipe (Delaglio et al., 1995) and analyzed using CcpNMR-Analysis (Vranken et al., 2005). Proton chemical shifts were referenced directly to internal DSS at 0.00 ppm, with heteronuclei referenced indirectly by relative gyromagnetic ratios.

Assignments and Structure Calculation

Assignments were performed in a combined automatic and manual process aided by Autoassign (Zimmerman et al., 1997). NOESY peaks were manually picked in CcpNMR. Torsion angle restraints were from TALOS (Cornilescu et al., 1999). The three-dimensional structures were calculated by a combination of automated NOESY peak assignment and torsion angle dynamics implemented in CYANA (Güntert, 2003), as well as manual inspection and assignments. The standard CYANA procedure of seven cycles of NOE assignment and structure calculation was performed. Initially, 100 randomized conformers were generated and subjected to 10,000 torsion angle dynamic steps, and selecting 20 structures with the lowest target function value between runs. Iteratively, assignments were checked manually, modified if needed, and structures were recalculated. The final 250 structures were calculated using Xplor-NIH (Schwieters et al., 2003) on the basis of the lowest-energy structure from CYANA with the assigned NOEs and TALOS dihedral angles as restraints. The secondary structure content was analyzed using DSSP. A set of 10 lowest energy/no-violation structures were chosen to represent the final structure and were refined in explicit water using ARIA2 (Rieping et al., 2007).

^{15}N Relaxation

The ^{15}N spin relaxation experiments included determination of the longitudinal (R_1) and transverse (R_2) relaxation rate constants and were recorded using a standard HSQC sequence (Farrow et al., 1994) at a 750 MHz proton frequency field. The relaxation decays were measured using seven (0, 0.2, 0.4, 0.6, 0.6, 0.8, 1.0, and 1.2 s) and six (0.01, 0.03, 0.05, 0.07, 0.09, and 0.11 s) different relaxation delays for R_1 and R_2. The number of transients was 256 for hPRLR-D2 and 128 for hPRLR-D2^{I146L} experiments. The sweep width in the indirect dimension was minimized to allow for only 32 increments with a recovery delay of 1.5 s. The relaxation decays were fitted to single exponentials, and relaxation rates were determined. The samples were 0.5 mM and and 0.45 mM for ^{15}N-hPRLR-D2 and ^{15}N-hPRLR-D2^{I146L}, with buffers described as above. The overall correlation time for the rotational diffusion, τ_C, was estimated from the R_1 and R_2 values of residues in the β sheets using Tensor2 (Dosset et al., 2000).

Diffusion Measurements

Hydrodynamic radii were measured using PGSLED (Yao et al., 2000). The gradient strength was changed linearly from 500 to 30,000 G/cm in 25 steps with extra data points in the beginning. The signal intensity versus gradient strength was measured on the aromatic and the methyl groups separately and fitted to Gaussian decays. The hydrodynamic radius was calculated using the following equation from Wilkins et al. (1999):

$$Rh = \frac{d_\alpha Rh_\alpha}{d_{D2}},$$

with α-cyclodextrin as an internal reference, where d_α is the diffusion constant of α-cyclodextrin and d_{D2} that of hPRLR-D2 (or hPRLR-D2^{I146L}). Rh_α is the hydrodynamic radius of α-cyclodextrin (7.1 Å). All experiments were performed at 500 μM and 450 μM for hPRLR-D2 and hPRLR-D2^{I146L} in 10 mM Na_2HPO_4 (pH 7.4), 10 mM TCEP in 99.96% (v/v) D_2O, and 1 mM α-cyclodextrin at 25°C.

SAXS

SAXS-data on hPRLR-D2^{I146L} were recorded at the MAX-Lab synchrotron in Lund, Sweden, at beam line I711. Data were recorded at ~20°C, exposure time 180 s, wavelength 1 Å. Scattering from three different concentrations (1.1, 2.2, and 4.3 mg/ml) was collected in succession, each flanked by background (10 mM Na_2HPO_4, 10 mM TCEP [pH 7.4]) scattering measurements. Data from the lowest concentration hPRLR-D2^{I146L} sample were discarded due to low signal-to-noise ratio. The others were merged and used for further analysis. Data were processed using the ATSAS package (Konarev

et al., 2006). The hPRLR-D2 SAXS data were recorded at the HESYLAB synchrotron in Hamburg, Germany, at beam line X33 at three different concentrations (0.92, 1.9, and 3.85 mg/ml) in 10 mM Na_2HPO_4 and 10 mM TCEP (pH 7.4) at an exposure time of 30 s. Details are provided in the Supplemental Experimental Procedures.

Binding Analysis

Two [^{15}N,^{1}H]-HSQC spectra were recorded and compared, one of a 55 μM ^{15}N hPRLR-D2, and one of a 55 μM ^{15}N hPRLR-D2 and 435 μM unlabeled hPRL. This was repeated three times. In the reverse experiment, two HSQC spectra were recorded and compared; one of a 67 μM $^{13}C^{15}N$-hPRL sample and one of a 67 μM $^{13}C^{15}N$-hPRL and 135 μM unlabeled hPRLR-D2, all in 10% (v/v) D_2O, 10 mM NaH_2PO_4, and 0.02% (v/v) NaN_3 (pH 7.5).

CD Spectroscopy

Far-UV CD spectra were acquired from 200 nm to 250 nm at 20 nm/min, bandwidth 1 nm and 2 s response time at 25°C using a Jasco J-810 spectropolarimeter, 1 mm light path. 10 scans were averaged and buffers subtracted. Protein concentration was 5 μM in a 10 mM Na_2HPO_4 (pH 7.4).

Fluorescence Spectroscopy

Chemical denaturation by GuHCl was followed using a Perkin Elmer LS50B luminescence spectropolarimeter in a 5 mm quartz cuvette at room temperature. Titration series in the 0–6 M GuHCl range and 50 mM Na_2HPO_4, 10 mM TCEP (pH 7.4), and 5 μM protein with excitation at 280 nm with 5 nm slit widths were done. Emission was acquired from 300-400 nm, 100 nm/min, five scans averaged. The change in emission intensity at 342 nm with GuHCl concentration was fitted to a two-state model (Maxwell et al., 2005).

ACCESSION NUMBERS

The coordinates for the NMR solution structure of hPRLR-D2 have been deposited in the Protein Data Bank (http://www.rcsb.org) under the accession code 2LFG. Chemical shift assignments for hPRLR-D2 at pH 7.4 have been deposited in Biological Magnetic Resonance Bank (http://www.bmrb.wisc.edu/) under the accession number 17752.

SUPPLEMENTAL INFORMATION

Supplemental Information includes three figures, one table, and Supplemental Experimental Procedures and can be found with this article online at doi:10.1016/j.str.2011.12.010.

ACKNOWLEDGMENTS

This work was supported by the Danish Research Councils (grant #21040604 to B.B.K.), The Novo Nordisk Foundation (B.B.K.), the Danish Cancer Society (B.B.K.), ANR-07-PCVI-0029 (V.G.), and Novo Nordisk A/S. We thank Signe A. Sjørup for excellent technical assistance, Yngve Cerenius and Lise Arleth for SAXS data analysis support, and the Danish Instrument Center at the Carlsberg Research Center for spectrometer time.

Received: August 26, 2011
Revised: November 17, 2011
Accepted: December 12, 2011
Published: February 7, 2012

REFERENCES

Andersen, N.H., Olsen, K.A., Fesinmeyer, R.M., Tan, X., Hudson, F.M., Eidenschink, L.A., and Farazi, S.R. (2006). Minimization and optimization of designed beta-hairpin folds. J. Am. Chem. Soc. *128*, 6101–6110.

Bass, S.H., Mulkerrin, M.G., and Wells, J.A. (1991). A systematic mutational analysis of hormone-binding determinants in the human growth hormone receptor. Proc. Natl. Acad. Sci. USA *88*, 4498–4502.

Baumgartner, J.W., Wells, C.A., Chen, C.M., and Waters, M.J. (1994). The role of the WSXWS equivalent motif in growth hormone receptor function. J. Biol. Chem. *269*, 29094–29101.

Bogorad, R.L., Courtillot, C., Mestayer, C., Bernichtein, S., Harutyunyan, L., Jomain, J.B., Bachelot, A., Kuttenn, F., Kelly, P.A., Goffin, V., and Touraine, P.; Benign Breast Diseases Study Group. (2008). Identification of a gain-of-function mutation of the prolactin receptor in women with benign breast tumors. Proc. Natl. Acad. Sci. USA *105*, 14533–14538.

Broutin, I., Jomain, J.B., Tallet, E., van Agthoven, J., Raynal, B., Hoos, S., Kragelund, B.B., Kelly, P.A., Ducruix, A., England, P., and Goffin, V. (2010). Crystal structure of an affinity-matured prolactin complexed to its dimerized receptor reveals the topology of hormone binding site 2. J. Biol. Chem. *285*, 8422–8433.

Brown, R.J., Adams, J.J., Pelekanos, R.A., Wan, Y., McKinstry, W.J., Palethorpe, K., Seeber, R.M., Monks, T.A., Eidne, K.A., Parker, M.W., and Waters, M.J. (2005). Model for growth hormone receptor activation based on subunit rotation within a receptor dimer. Nat. Struct. Mol. Biol. *12*, 814–821.

Canbay, E., Degerli, N., Gulluoglu, B.M., Kaya, H., Sen, M., and Bardakci, F. (2004). Could prolactin receptor gene polymorphism play a role in pathogenesis of breast carcinoma? Curr. Med. Res. Opin. *20*, 533–540.

Carver, K.C., Arendt, L.M., and Schuler, L.A. (2009). Complex prolactin crosstalk in breast cancer: new therapeutic implications. Mol. Cell. Endocrinol. *307*, 1–7.

Clevenger, C.V., Gadd, S.L., and Zheng, J. (2009). New mechanisms for PRLr action in breast cancer. Trends Endocrinol. Metab. *20*, 223–229.

Cornilescu, G., Delaglio, F., and Bax, A. (1999). Protein backbone angle restraints from searching a database for chemical shift and sequence homology. J. Biomol. NMR *13*, 289–302.

Courtillot, C., Chakhtoura, Z., Bogorad, R., Genestie, C., Bernichtein, S., Badachi, Y., Janaud, G., Akakpo, J.P., Bachelot, A., Kuttenn, F., et al; Benign Breast Diseases Study Group. (2010). Characterization of two constitutively active prolactin receptor variants in a cohort of 95 women with multiple breast fibroadenomas. J. Clin. Endocrinol. Metab. *95*, 271–279.

Delaglio, F., Grzesiek, S., Vuister, G.W., Zhu, G., Pfeifer, J., and Bax, A. (1995). NMRPipe: a multidimensional spectral processing system based on UNIX pipes. J. Biomol. NMR *6*, 277–293.

Dosset, P., Hus, J.C., Blackledge, M., and Marion, D. (2000). Efficient analysis of macromolecular rotational diffusion from heteronuclear relaxation data. J. Biomol. NMR *16*, 23–28.

Duriez, B., Sobrier, M.L., Duquesnoy, P., Tixier-Boichard, M., Decuypere, E., Coquerelle, G., Zeman, M., Goossens, M., and Amselem, S. (1993). A naturally occurring growth hormone receptor mutation: in vivo and in vitro evidence for the functional importance of the WS motif common to all members of the cytokine receptor superfamily. Mol. Endocrinol. *7*, 806–814.

Farrow, N.A., Muhandiram, R., Singer, A.U., Pascal, S.M., Kay, C.M., Gish, G., Shoelson, S.E., Pawson, T., Forman-Kay, J.D., and Kay, L.E. (1994). Backbone dynamics of a free and phosphopeptide-complexed Src homology 2 domain studied by 15N NMR relaxation. Biochemistry *33*, 5984–6003.

Gadd, S.L., and Clevenger, C.V. (2006). Ligand-independent dimerization of the human prolactin receptor isoforms: functional implications. Mol. Endocrinol. *20*, 2734–2746.

García De La Torre, J., Huertas, M.L., and Carrasco, B. (2000). Calculation of hydrodynamic properties of globular proteins from their atomic-level structure. Biophys. J. *78*, 719–730.

Goffin, V., Binart, N., Touraine, P., and Kelly, P.A. (2002). Prolactin: the new biology of an old hormone. Annu. Rev. Physiol. *64*, 47–67.

Goffin, V., Bernichtein, S., Touraine, P., and Kelly, P.A. (2005). Development and potential clinical uses of human prolactin receptor antagonists. Endocr. Rev. *26*, 400–422.

Goffin, V., Hoang, D.T., Bogorad, R.L., and Nevalainen, M.T. (2011). Prolactin regulation of the prostate gland: a female player in a male game. Nature Rev. *8*, 597–607.

Gourdou, I., Gabou, L., Paly, J., Kermabon, A.Y., Belair, L., and Djiane, J. (1996). Development of a constitutively active mutant form of the prolactin

receptor, a member of the cytokine receptor family. Mol. Endocrinol. *10*, 45–56.

Güntert, P. (2003). Automated NMR protein structure calculation. Prog. Nucl. Magn. Reson. Spectrosc. *43*, 105–125.

Hecht, O., Dingley, A.J., Schwanter, A., Ozbek, S., Rose-John, S., and Grötzinger, J. (2006). The solution structure of the membrane-proximal cytokine receptor domain of the human interleukin-6 receptor. Biol. Chem. *387*, 1255–1259.

Hilton, D.J., Watowich, S.S., Katz, L., and Lodish, H.F. (1996). Saturation mutagenesis of the WSXWS motif of the erythropoietin receptor. J. Biol. Chem. *271*, 4699–4708.

Jomain, J.B., Tallet, E., Broutin, I., Hoos, S., van Agthoven, J., Ducruix, A., Kelly, P.A., Kragelund, B.B., England, P., and Goffin, V. (2007). Structural and thermodynamic bases for the design of pure prolactin receptor antagonists: X-ray structure of Del1-9-G129R-hPRL. J. Biol. Chem. *282*, 33118–33131.

Jorge, A.A., Souza, S.C., Arnhold, I.J., and Mendonca, B.B. (2004). The first homozygous mutation (S226I) in the highly-conserved WSXWS-like motif of the GH receptor causing Laron syndrome: supression of GH secretion by GnRH analogue therapy not restored by dihydrotestosterone administration. Clin. Endocrinol. (Oxf.) *60*, 36–40.

Kernebeck, T., Pflanz, S., Müller-Newen, G., Kurapkat, G., Scheek, R.M., Dijkstra, K., Heinrich, P.C., Wollmer, A., Grzesiek, S., and Grötzinger, J. (1999). The signal transducer gp130: solution structure of the carboxy-terminal domain of the cytokine receptor homology region. Protein Sci. *8*, 5–12.

Kline, J.B., Rycyzyn, M.A., and Clevenger, C.V. (2002). Characterization of a novel and functional human prolactin receptor isoform (deltaS1PRLr) containing only one extracellular fibronectin-like domain. Mol. Endocrinol. *16*, 2310–2322.

Konarev, P.V., Petoukhov, M.V., Volkov, V.V., and Svergun, D.I. (2006). *ATSAS* 2.1, a program package for small-angle scattering data analysis. J. Appl. Crystallogr. *39*, 277–286.

Kulkarni, M.V., Tettamanzi, M.C., Murphy, J.W., Keeler, C., Myszka, D.G., Chayen, N.E., Lolis, E.J., and Hodsdon, M.E. (2010). Two independent histidines, one in human prolactin and one in its receptor, are critical for pH-dependent receptor recognition and activation. J. Biol. Chem. *285*, 38524–38533.

Liu, W., and Brooks, C.L. (2011). Functional impact of manipulation on the relative orientation of human prolactin receptor domains. Biochemistry *50*, 5333–5344.

Man, D., He, W., Sze, K.H., Gong, K., Smith, D.K., Zhu, G., and Ip, N.Y. (2003). Solution structure of the C-terminal domain of the ciliary neurotrophic factor (CNTF) receptor and ligand free associations among components of the CNTF receptor complex. J. Biol. Chem. *278*, 23285–23294.

Maxwell, K.L., Wildes, D., Zarrine-Afsar, A., De Los Rios, M.A., Brown, A.G., Friel, C.T., Hedberg, L., Horng, J.C., Bona, D., Miller, E.J., et al. (2005). Protein folding: defining a "standard" set of experimental conditions and a preliminary kinetic data set of two-state proteins. Protein Sci. *14*, 602–616.

Mulhern, T.D., Lopez, A.F., D'Andrea, R.J., Gaunt, C., Vandeleur, L., Vadas, M.A., Booker, G.W., and Bagley, C.J. (2000). The solution structure of the cytokine-binding domain of the common beta-chain of the receptors for granulocyte-macrophage colony-stimulating factor, interleukin-3 and interleukin-5. J. Mol. Biol. *297*, 989–1001.

Narhi, L.O., Aoki, K.H., Philo, J.S., and Arakawa, T. (1997). Changes in conformation and stability upon formation of complexes of erythropoietin (EPO) and soluble EPO receptor. J. Protein Chem. *16*, 213–225.

Nevalainen, M.T., Valve, E.M., Ingleton, P.M., Nurmi, M., Martikainen, P.M., and Harkonen, P.L. (1997). Prolactin and prolactin receptors are expressed and functioning in human prostate. J. Clin. Invest. *99*, 618–627.

Neville, M.C., McFadden, T.B., and Forsyth, I. (2002). Hormonal regulation of mammary differentiation and milk secretion. J. Mammary Gland Biol. Neoplasia *7*, 49–66.

Ozbek, S., Grötzinger, J., Krebs, B., Fischer, M., Wollmer, A., Jostock, T., Müllberg, J., and Rose-John, S. (1998). The membrane proximal cytokine receptor domain of the human interleukin-6 receptor is sufficient for ligand binding but not for gp130 association. J. Biol. Chem. *273*, 21374–21379.

Rieping, W., Habeck, M., Bardiaux, B., Bernard, A., Malliavin, T.E., and Nilges, M. (2007). ARIA2: automated NOE assignment and data integration in NMR structure calculation. Bioinformatics *23*, 381–382.

Robertson, F.G., Harris, J., Naylor, M.J., Oakes, S.R., Kindblom, J., Dillner, K., Wennbo, H., Törnell, J., Kelly, P.A., Green, J., and Ormandy, C.J. (2003). Prostate development and carcinogenesis in prolactin receptor knockout mice. Endocrinology *144*, 3196–3205.

Rozakis-Adcock, M., and Kelly, P.A. (1992). Identification of ligand binding determinants of the prolactin receptor. J. Biol. Chem. *267*, 7428–7433.

Rui, H., Kirken, R.A., and Farrar, W.L. (1994). Activation of receptor-associated tyrosine kinase JAK2 by prolactin. J. Biol. Chem. *269*, 5364–5368.

Schwieters, C.D., Kuszewski, J.J., Tjandra, N., and Clore, G.M. (2003). The Xplor-NIH NMR molecular structure determination package. J. Magn. Reson. *160*, 65–73.

Svensson, L.A., Bondensgaard, K., Nørskov-Lauritsen, L., Christensen, L., Becker, P., Andersen, M.D., Maltesen, M.J., Rand, K.D., and Breinholt, J. (2008). Crystal structure of a prolactin receptor antagonist bound to the extracellular domain of the prolactin receptor. J. Biol. Chem. *283*, 19085–19094.

Tallet, E., Fernandez, I., Zhang, C., Salsac, M., Gregor, N., Ayoub, M.A., Pin, J.P., Trinquet, E., and Goffin, V. (2011). Investigation of prolactin receptor activation and blockade using time-resolved fluorescence resonance energy transfer. Frontiers in Cellular Endocrinology *2*, 1–17.

Tan, D., Huang, K.T., Ueda, E., and Walker, A.M. (2008). S2 deletion variants of human PRL receptors demonstrate that extracellular domain conformation can alter conformation of the intracellular signaling domain. Biochemistry *47*, 479–489.

Teilum, K., Brath, U., Lundström, P., and Akke, M. (2006). Biosynthetic 13C labeling of aromatic side chains in proteins for NMR relaxation measurements. J. Am. Chem. Soc. *128*, 2506–2507.

Teilum, K., Hoch, J.C., Goffin, V., Kinet, S., Martial, J.A., and Kragelund, B.B. (2005). Solution structure of human prolactin. J. Mol. Biol. *351*, 810–823.

Vaclavicek, A., Hemminki, K., Bartram, C.R., Wagner, K., Wappenschmidt, B., Meindl, A., Schmutzler, R.K., Klaes, R., Untch, M., Burwinkel, B., and Försti, A. (2006). Association of prolactin and its receptor gene regions with familial breast cancer. J. Clin. Endocrinol. Metab. *91*, 1513–1519.

van Agthoven, J., Zhang, C., Tallet, E., Raynal, B., Hoos, S., Baron, B., England, P., Goffin, V., and Broutin, I. (2010). Structural characterization of the stem-stem dimerization interface between prolactin receptor chains complexed with the natural hormone. J. Mol. Biol. *404*, 112–126.

Vranken, W.F., Boucher, W., Stevens, T.J., Fogh, R.H., Pajon, A., Llinas, M., Ulrich, E.L., Markley, J.L., Ionides, J., and Laue, E.D. (2005). The CCPN data model for NMR spectroscopy: development of a software pipeline. Proteins *59*, 687–696.

Weidemann, T., Höfinger, S., Müller, K., and Auer, M. (2007). Beyond dimerization: a membrane-dependent activation model for interleukin-4 receptor-mediated signalling. J. Mol. Biol. *366*, 1365–1373.

Wilkins, D.K., Grimshaw, S.B., Receveur, V., Dobson, C.M., Jones, J.A., and Smith, L.J. (1999). Hydrodynamic radii of native and denatured proteins measured by pulse field gradient NMR techniques. Biochemistry *38*, 16424–16431.

Wu, L., McElheny, D., Huang, R., and Keiderling, T.A. (2009). Role of tryptophan-tryptophan interactions in Trpzip beta-hairpin formation, structure, and stability. Biochemistry *48*, 10362–10371.

Yamasaki, K., Naito, S., Anaguchi, H., Ohkubo, T., and Ota, Y. (1997). Solution structure of an extracellular domain containing the WSxWS motif of the granulocyte colony-stimulating factor receptor and its interaction with ligand. Nat. Struct. Biol. *4*, 498–504.

Yamazaki, T., Forman-Kay, J.D., and Kay, L.E. (1993). Two-dimensional NMR experiments for correlating carbon-13.beta. and proton.delta./.epsilon. chemical shifts of aromatic residues in 13C-labeled proteins via scalar couplings. J. Am. Chem. Soc. *115*, 11054–11055.

Yao, S., Howlett, G.J., and Norton, R.S. (2000). Peptide self-association in aqueous trifluoroethanol monitored by pulsed field gradient NMR diffusion measurements. J. Biomol. NMR *16*, 109–119.

Yoshimura, A., Zimmers, T., Neumann, D., Longmore, G., Yoshimura, Y., and Lodish, H.F. (1992). Mutations in the Trp-Ser-X-Trp-Ser motif of the erythropoietin receptor abolish processing, ligand binding, and activation of the receptor. J. Biol. Chem. *267*, 11619–11625.

Zimmerman, D.E., Kulikowski, C.A., Huang, Y., Feng, W., Tashiro, M., Shimotakahara, S., Chien, C.-y., Powers, R., and Montelione, G.T. (1997). Automated analysis of protein NMR assignments using methods from artificial intelligence. J. Mol. Biol. *269*, 592–610.

